

Compact expansion of a repulsive suspension

Matan Yah Ben Zion¹ and Naomi Oppenheimer^{1,*}

¹*School of Physics and the Center for Physics and Chemistry of Living Systems, Tel Aviv University, Tel Aviv 6997801, Israel*
(Dated: August 4, 2023)

Short-range repulsion governs the dynamic behavior of matter across length scales, from atoms to animals. As the density increases, the dynamics transition from nearest-neighbor to many-body interactions, posing a challenge for an analytical description. Here we use theory, simulations, and experiments to show that a suspension of particles with short-range repulsion spreads compactly. Unlike the diffusive boundary of a spreading drop of Brownian particles, a compact expansion is characterized by a density profile that is strictly zero beyond a cutoff distance. Starting from the microscopic interactions, we derive an effective, non-linear diffusion equation and find that the dynamics exhibit two distinct transitions: (1) when very dense, particle-particle interactions extend beyond nearest neighbors, and the ensemble grows in a self-similar fashion as $t^{1/4}$. (2) at lower densities, nearest-neighbor interactions dominate, and the expansion slows to logarithmic growth. We examine the second regime experimentally by monitoring the expansion of a dense suspension of charge-stabilized colloids. Using simulations of thousands of particles, we observe the continuous crossover between the self-similar and the logarithmic dynamics. Our results are general and robust, with practical implications in engineering and pharmaceutical industries, where suspensions must operate at extreme densities.

INTRODUCTION

Suspensions are everywhere — from the ink we (used to) write with, the soy milk we drink, and the drugs we consume to the very structure of most living systems. Life is built on repulsive interactions in keeping microscopic particles suspended. More often than not, the particles are charged, and electrostatic interactions are screened by the presence of ions in solution [1–4]. Such is the case for charged proteins in a membrane [5–8], vesicles in suspension [9, 10], droplets in microfluidic devices [11], water purification, plasma physics, and high charge-density batteries [12–14]. In other cases, particles are not strictly charged, yet are repelled by short-range forces, e.g., globular polymers, or colloidal particles coated by a brush shell, and sub-atomic particles interacting in the nucleus [15–19].

Short-range repulsion is crucial for interactions spanning a wide spectrum of sizes and dynamics. These include the packing and flow of granular materials like sand or seeds [20]. It is also used to describe biological systems, elucidating the motion of bacterial colonies [21, 22], the collective behavior of insect swarms such as ants [23], and bees [24], or the coordinated movement of vertebrates in herds, schools, flocks [25], as well as for human crowds [26–28]. Furthermore, short-range repulsion is often utilized in modeling non-equilibrium many-body systems [29–34], in information theory [35], and in swarm robotics [36, 37].

In what follows, we consider the expansion of a suspension of particles with repulsive, short-range interactions that dominate over thermal diffusion. We find that when the interaction has a typical decay length, the suspension expands compactly — the concentration vanishes identically outside a core of finite size. Compact profiles are

found in diverse physical systems, including gas diffusion through porous medium [38, 39], thin films with a free surface [40, 41], and even in population dynamics [42]. A family of compact solitons (called compactons) were found as solutions to a generalization of the Korteweg-De Vrie (KdV) equation [43]. These systems were modeled using a continuum, hydrodynamic description, characterized by phenomenological parameters. Here we show analytically, starting from a microscopic basis, that a non-linear diffusion equation with a compact solution is generic for particles with short-range repulsion. We find under what conditions the continuum description breaks down, leading to a crossover in the dynamics.

As we outline below, at high densities, the time evolution and distribution of the density field $n(\mathbf{r}, t)$, are determined by a non-linear diffusion equation, stemming from particle-particle interactions, leading to a concentration-dependent diffusion of the form

$$\frac{\partial n}{\partial t} = \nabla \cdot [D(n)\nabla n] = D(n)\nabla^2 n + \alpha|\nabla n|^2, \quad (1)$$

where we define $D(n) \equiv \alpha n$, which takes the role of an effective density-dependent diffusion coefficient. Unlike the usual sense of a diffusion coefficient stemming from random motion, here $D(n)$ is associated with the response to a density variation, and α is derived from the microscopic pair potential. Since the effective diffusion coefficient, $D(n)$ is proportional to the density, particles at the drop's boundary have a lower diffusion constant than particles at the center. The solutions are inherently different from regular diffusion. For example, for diffusion, there is a Gaussian spread of the density. Here, in the two-dimensional (2D) case we consider, the density profile at high concentrations is parabolic and is strictly zero beyond a maximal radius which grows with time. In this

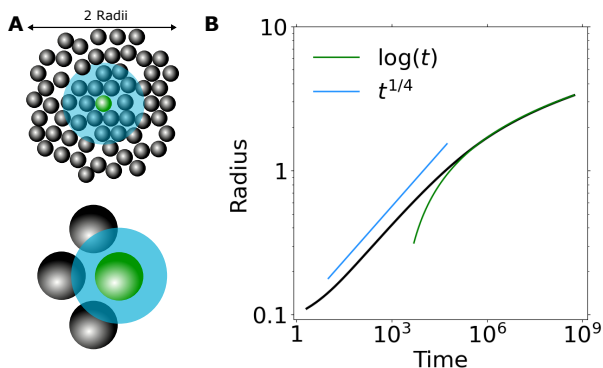


FIG. 1. (a) Schematics of the interaction of repulsive particles with short-range repulsion in the dense region (top), where each particle interacts with many others indicated in blue, and in the semi-sparse region (bottom), where a particle interacts only with its nearest neighbors. (b) simulation of 10,000 particles starting from a dense random distribution. At early times, each particles interact with many others and we see the $R \sim t^{1/4}$ scaling predicted by the self-similar solution. At long times, each particle interacts only with its nearest neighbors and there is a transition to the semi-sparse limit with a logarithmic dependence on time.

limit, unlike classic diffusion, the radius of the drop does not grow as the square root of time but as $t^{1/4}$. At lower concentrations, when the distance between particles is larger than the characteristic repulsive distance, particle interactions are dominated by nearest neighbors. We show that in this limit, the suspension spreads logarithmically with time.

The expansion of the repulsive suspension can be described by the time evolution of its radius. For the ubiquitous exponential or screened electrostatic interactions, the asymptotic limits of the time evolution are given by

$$R(t) \propto \begin{cases} t^{1/4} & \text{if } n \gg 1 \\ \log(t) & \text{if } n \ll 1 \end{cases}, \quad (2)$$

where $n = \rho/\rho_c$ is the non-dimensionalized density, $\rho_c \equiv 1/(\pi l^2)$, with l being the typical decay length of the short-range repulsion. The transition from the two types of expansions occurs when the typical distance between particles, L is equal to the decay length, l . Our analysis addresses the athermal limit, where Brownian motion is negligible. This is valid when $D = \alpha n \gg D_0$ where D_0 is the self-diffusion coefficient originating from thermal fluctuations. Similarly, this is true when the distance between particles satisfies $L \ll \sqrt{F_0 l^3/k_B T}$, where F_0 is the strength of the repulsive force, k_B is Boltzmann constant, and T is temperature. Note that in the overdamped dynamics discussed here, this limit is independent of viscosity, which plays a dual role in both the deterministic and stochastic forces.

Equations 1 and 2 are the main results of this work, which is structured as follows: first, we derive the two

regimes analytically. Next, we compare analytic results with simulations and experiments. We show that at high densities ($n \gg 1$), where interactions go beyond nearest neighbors, both numerical integration of the mass conservation equation, as well as discrete simulations using the pair interactions, are quantitatively consistent with the approximate analytical solution; then we proceed to show that in the semi-sparse limit, where interactions are dominated by nearest neighbors, ($n \leq 1$) indeed the dynamics follow Eq. 2 as observed in both experiments of a concentrated charged colloidal suspension and discrete simulations.

RESULTS

Governing Equations

We examine particles in the overdamped limit, where inertia is negligible, and the force, \mathbf{F} and velocity \mathbf{v} , are proportional through constant mobility, $\mathbf{v} = \mu \mathbf{F}$. Individual particles follow deterministic dynamics (no Brownian motion) and interact through a pair interaction, $F(r)$. The interaction can be due to any short-ranged, isotropic, repulsive force — from sub-atomic Yukawa potential, through Pauli repulsion at the inter-atomic scale, screened Coulomb potential in an ionic solution, plasma, or even soft-core entropic repulsion in colloidal suspensions [13, 15, 44–46]. Most of our results are generic, and for simplicity, we consider two-dimensional exponential interactions in the main text, $F(r) = v_0/\mu e^{-r/l}$. In the Supplementary Information (SI), we show results for screened-electrostatics (see also Table I).

To build intuition, let us start by examining a single particle, then two, and then many. For a single Brownian particle, the mean-square displacement grows as \sqrt{t} . By contrast, a single repulsive, athermal particle, is stationary. Unlike the separation between two Brownian particles that diffuse apart at a rate of \sqrt{t} , two athermal, strictly repulsive particles separate as $\sim \log(t)$ since $dr/dt = 2v_0 e^{-r/l}$, where v_0 is the magnitude of the velocity given by $v_0 = \mu F_0$. In an ensemble of many repulsive particles, each particle moves by the sum of the interaction from all particles. That is, the velocity of particle i is given by,

$$\mathbf{v}_i(\mathbf{r}_i) = \sum_j \frac{1}{\mu} F\left(\frac{r_{ij}}{l}\right) \hat{\mathbf{r}}_{ij} = \sum_j v_0 e^{-r_{ij}/l} \hat{\mathbf{r}}_{ij}, \quad (3)$$

where $\mathbf{r}_{ij} = \mathbf{r}_i - \mathbf{r}_j$, $r_{ij} = |\mathbf{r}_{ij}|$, and $\hat{\mathbf{r}}_{ij} = \mathbf{r}_{ij}/r_{ij}$. Discrete simulations of Eq. 3 (see Fig. 1) show that the radius of an ensemble of N repulsive particles grows as $R \sim t^{1/4}$ in the dense limit ($n \gg 1$) and as $\log(t)$ in the semi-sparse limit ($n \leq 1$). In both cases the expansion is sub-diffusive. The semi-sparse limit is closer to the two particle scenario, but the dense limit is different. When

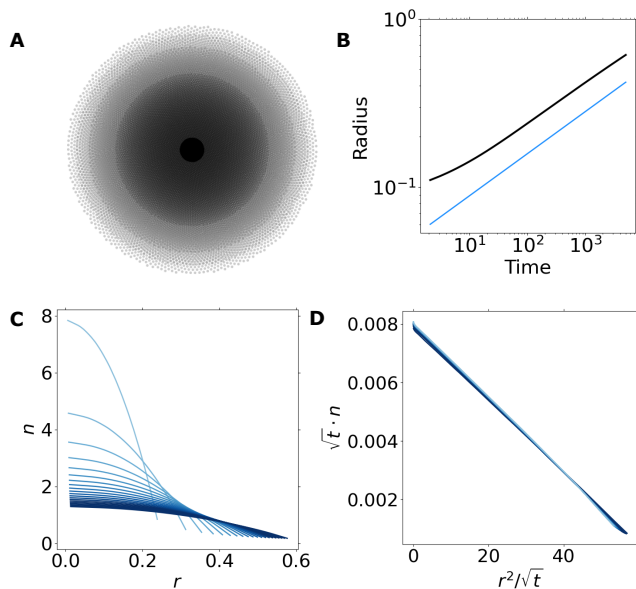


FIG. 2. Simulations of repulsive particles at high density show self-similar profile, as predicted in the continuum limit. Results from a simulation of 10,000 particles with exponentially repulsive interactions. We start from a high density and track the particles as they spread. a) Snapshots of the simulations at different times ($t = 0, 5,000, 20,000, 35,000, 50,000$). b) Radius as a function of time showing the $t^{1/4}$ scaling. c) Density as a function of radius for different times. Color goes from bright to dark as time progresses. d) Re-scaled density $\sqrt{t}n$ as a function of r^2/\sqrt{t} showing all the curves collapse to a single line as predicted by Eq. 12.

does the two-particle case transition to the continuum description? We will now derive analytically the crossover between these two limits.

Analytic Results in the Dense Limit. In the dense limit, $n \gg 1$, we coarse-grain the velocity to derive a diffusion equation. The following procedure is analogous to a Fokker-Planck expansion with a mean-field closure [47–50]. We start with the mass conservation equation for the number of particles

$$\frac{\partial n}{\partial t} + \nabla \cdot (n\mathbf{v}) = 0, \quad (4)$$

where n is the normalized density of particles such that $n = \rho/\rho_c$, $\rho(\mathbf{r}(t)) = \sum_i \delta(\mathbf{r}(t) - \mathbf{r}_i(t))$ [and $\rho_c \equiv 1/(\pi l^2)$ with l being the decay of the repulsive interactions]. We turn to find the coarse-grained velocity, $\mathbf{v}(\mathbf{r}(t))$. Since the interactions are purely repulsive, the velocity field is of the form $\mathbf{v}(\mathbf{r}) = v(r)\hat{r}$ [51], where $v(r)$ is given by the short-ranged repulsive force felt from all other particles. In the limit of a continuous density of particles, Eq. 3

becomes

$$\mathbf{v}(\mathbf{X}) = \frac{\rho_c}{\mu} \int_0^R \int_0^{2\pi} n(\mathbf{Y}) \frac{\mathbf{X} - \mathbf{Y}}{|\mathbf{X} - \mathbf{Y}|} F\left(\frac{|\mathbf{X} - \mathbf{Y}|}{l}\right) d^d \mathbf{Y}, \quad (5)$$

where d is the dimension. Equation 5 is the velocity at position \mathbf{X} due to all the forces coming from the other particles. The forces are aligned along the particle-particle separation distance such that $\hat{r}_{ij} \rightarrow (\mathbf{X} - \mathbf{Y})/|\mathbf{X} - \mathbf{Y}|$. Combined with the mass conservation, Eq. 4, the two equations can be solved numerically. Using an approximation, we can continue analytically by recalling the short range nature of the interaction.

In principle, the integration boundaries depend on the position of the particle \mathbf{X} , but distances $|\mathbf{X} - \mathbf{Y}| \gg l$ will hardly contribute due to the short-ranged nature of the forces. For particles away from the edge of the suspension, $|R - X| \gg l$, we can extend the integration boundaries to the entire space. Thus the velocity is approximately

$$\mathbf{v}(\mathbf{X}) \approx -\frac{1}{\pi\mu} \int n(\mathbf{X} + l\mathbf{s}) \hat{s} F(|s|) d^d \mathbf{s}, \quad (6)$$

where we have changed integration variables to a normalized distance $\mathbf{s} = (\mathbf{Y} - \mathbf{X})/l$. In 2D polar coordinates $\mathbf{s} = r\hat{s} = r(\cos\theta, \sin\theta)$, $\mathbf{X} = r'(\cos\phi, \sin\phi)$, with $\theta, \phi \in (0, 2\pi)$ and $r \in (0, \infty)$. A multipole expansion of Eq. 6 in the density gives the Taylor series,

$$n(\mathbf{X} + l\mathbf{s}) \approx n(\mathbf{X}) + l\mathbf{s} \cdot \nabla n(\mathbf{X}) + \dots \quad (7)$$

By symmetry, the first term of the moment expansion in Eq. 7 vanishes after integration in Eq. 6. The remaining leading term in the velocity is the concentration gradient,

$$\begin{aligned} \mathbf{v}(\mathbf{X}) &\approx -\frac{l}{\pi\mu} \nabla n(\mathbf{X}) \cdot \int \mathbf{s} \hat{s} F(r) d^d \mathbf{s} \\ &= -\frac{l}{\pi\mu} \nabla n(\mathbf{X}) \cdot \int \hat{s} \hat{s} d\Omega \int r^d F(r) dr \\ &= -\alpha \frac{\partial n}{\partial r} \hat{r}, \end{aligned} \quad (8)$$

where $d\Omega$ signifies angular integration. In both screened Coulomb and exponential repulsion in 2D $\alpha = 2v_0 l$. Table I shows a few coefficients for different dimensions and forces.

The full non-linear diffusion equation (Eq. 1) is found when plugging the velocity approximation (Eq. 8) in the equation for mass conservation (Eq. 4), giving an effective diffusion coefficient that linearly increases with density, $D = \alpha n(r)$, which takes the following form in polar coordinates:

$$\frac{\partial n}{\partial t} - \frac{\alpha}{r} \frac{\partial}{\partial r} \left(r n \frac{\partial n}{\partial r} \right) = 0. \quad (9)$$

Force	$\frac{\mu}{v_0} F(r)$	$\frac{1}{v_0 l} \alpha_{2D}$	$\frac{1}{v_0 l} \alpha_{3D}$
Exponential	e^{-r}	2	8
Screened	$\frac{1}{r} e^{-r} \left(1 + \frac{1}{r}\right)$	2	4
Gaussian	e^{-r^2}	$\frac{\sqrt{\pi}}{4}$	$\frac{2}{3}$

TABLE I. Coefficients of the approximate velocity in 2D and 3D for different forces — exponential, screened electrostatics and Gaussian.

This equation is identical to the effective porous media equation [38] but derived from the details of the pair interaction, allowing us to trace the effective parameters to their microscopic origins. Self-similar solutions are given by dimensional analysis of Eq. 9 (here we follow Refs. [40, 41]): We start by assuming a solution of the form $n = At^\gamma f(Br/t^\beta) = At^\gamma f(\eta)$. We can further link γ and β by recalling that the total number of particles, N , is independent of time

$$N = \rho_c \int n(r) r dr d\theta \propto t^{\gamma+2\beta} \int f(\eta) \eta d\eta. \quad (10)$$

which is constant only for $\gamma = -2\beta$. The density therefore has the form $n = At^{-2\beta} f(Br/t^\beta)$. Placing n in Eq. 9, we find that f is indeed a function of η alone (as was assumed), and we must have $\beta = \frac{1}{4}$, and $B^2 = \frac{1}{8A\alpha}$. The equation for the self-similarity function, f , is

$$2f + \eta f' = -\frac{1}{2\eta} \frac{d}{d\eta} (\eta f f'), \quad (11)$$

whose solution is parabolic, such that the concentration is

$$n = \frac{A}{\sqrt{t}} (1 - \eta^2) = \frac{A}{\sqrt{t}} \left(1 - B^2 \frac{r^2}{\sqrt{t}}\right). \quad (12)$$

Finally, the prefactor, A , is determined from the total number of particles (Eq. 10), giving $A = \sqrt{3N/(8\pi\rho_c\alpha)}$. The self-similar profile is quadratic with respect to η hence it is quadratic with respect to distance, and its width is an increasing function of time. Note that the concentration of particles is *strictly zero* beyond $Br = t^{1/4}$, meaning that the drop is compact. A similar calculation in 3D leads to $n = At^{-3/5} f(Br/t^{1/5})$.

Analytic Results in the Semi-Sparse Limit.

When the average distance between particles is larger than the decay length of the repulsive force, l , we can assume only nearest neighbors contribute to the interaction, and the discrete nature of the suspension cannot be ignored. In such cases, we can no longer use Eq. 8 in order to find the density as a function of time. However, we can still approximate the radius of the drop as it spreads by considering the velocity of particles at the edge. Due to the repulsive interactions, the arrangement

of particles is roughly hexagonal as verified in the simulations. We can assume a particle at the edge of the drop has three equally spaced nearest neighbors. Due to the isotropic nature of the interactions we can consider any particle. Without loss of generality, we take the particle positioned at $\mathbf{r} = R\hat{x}$. The particle will move with velocity $\mathbf{v}(R\hat{x}) = \frac{dR(t)}{dt} \hat{x} = 2v_0 e^{-R\sqrt{\pi/N}/l} \hat{x}$, where $R\sqrt{\pi/N}$ is the average distance between particles in the ensemble. The approximate radius is simply found by integrating the velocity

$$R(t) = \sqrt{\frac{N}{\pi}} l \log(t/t_0 + c), \quad (13)$$

with $t_0 = \sqrt{N/\pi} l / 2v_0$ and $c = \exp(\sqrt{R_0^2 \pi / l^2 N})$ where R_0 is the initial radius. We next demonstrate the validity of this result in simulations and experiments of a suspension of charge-stabilized colloids in deionized water.

Dense Limit Verification

Discrete Simulation in the Dense Limit. We ran simulations of 10,000 particles with short-ranged exponential repulsion. We start from a random configuration in a circle of size R and let the system evolve over time. As the drop evolves, it spreads, such that $R = R(t)$. We find the local density of particles by finding the Voronoi tessellation and calculating the area of each cell, A_{cell}^i [33]. The density is given by $n(r) = 1/A_{\text{cell}}^i$. The upper left panel in Fig. 2 shows overlaid snapshots from the simulation at different times. Figure 2B shows the radius of the drop as a function of time. After a short transient, the radius follows the expected power-law of $R \propto t^{1/4}$. The density profile as a function of the radius of the drop, r , at different times is presented in Fig. 2C. And lastly, the bottom right panel shows the rescaled density $\sqrt{t} n$ versus r^2/\sqrt{t} excluding the first few timesteps. Note how all the curves collapse to a single straight line according to the scaling of Eq. 12.

Numerical Solutions in the Dense Limit. To test the validity of the asymptotic solution, we numerically integrated the mass conservation equation, Eq. 4 together with the full velocity given by Eq. 5. Note that this is a numerical solution of the *full* partial differential equations. That is, without resorting to any of the assumptions used to derive Eq. 6 and the nonlinear diffusion equation, Eq. 9. Namely, without the asymptotic approximation of the integral in Eq. 5, and using the full density distribution (which now includes all terms in the Taylor expansion). To that end, we started with a narrow Gaussian distribution and propagated it in time. Further note that, unlike the discrete simulations, here, the initial distribution is not compact. The numerical results are presented in Fig. 3. On the left bottom panel, the density as a function of radius is presented at various

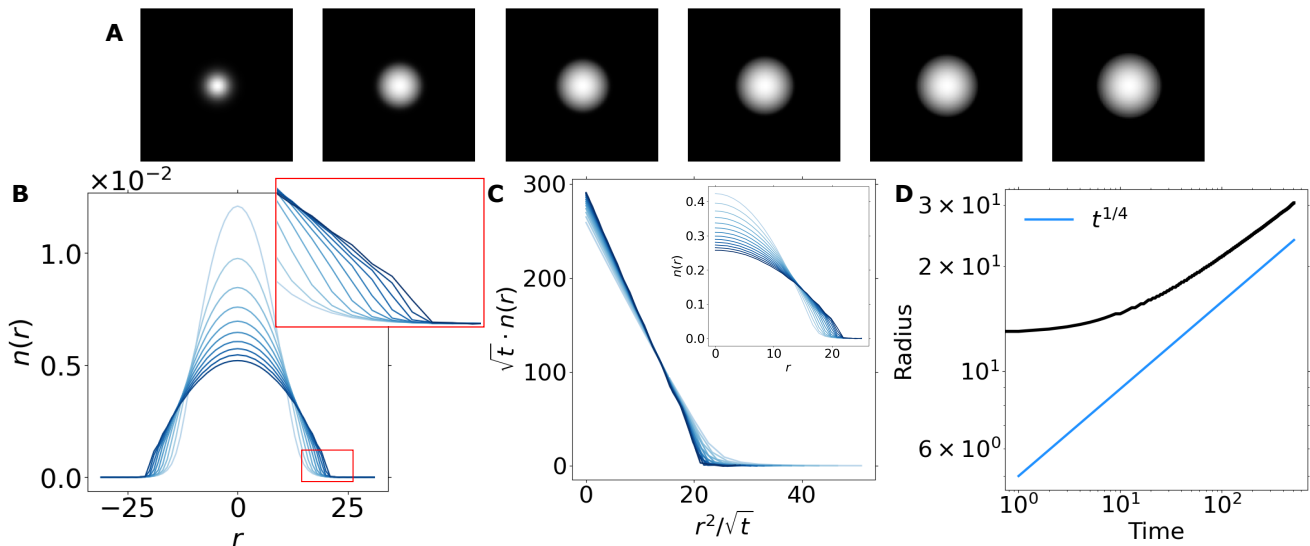


FIG. 3. Full numerical solution of Eq. 4 combined with Eq. 5 using Fast Fourier Transform with padded arrays. a) Snapshots of the density distribution at constant time intervals show that a repulsive suspension starting with an initially smooth Gaussian distribution spreads compactly. b) Radially averaged density profile as a function of the radius of the drop at different times. Inset shows a zoom-in on the edge of the drop, showing the sharpening of the cusp over time. Color goes from bright to dark as time progresses. c) Collapsed plot of the re-scaled distributions at later times (following Eq. 12). Density is scaled by \sqrt{t} and plotted against $\eta = r^2/\sqrt{t}$ as predicted by Eq. 12 for the approximate velocity, Eq. 8. Inset shows a plot of the density versus distance used for the figure. d) Radius as a function of time showing the expected growth as $t^{1/4}$.

times. The inset shows a zoom-in on the edge of the drop, showing that a cusp is formed at later times, indicating the solution's compactness. In the bottom-middle panel, the normalized density $\sqrt{t}n(r)$ is plotted as a function of r^2/\sqrt{t} , where a collapse of all later times to a single straight line is obtained, as expected from the nonlinear diffusion equation (Eq. 12). Lastly, on the right-bottom panel, the radius as a function of time shows the expected power-law of $\propto t^{1/4}$.

Semi-Sparse Limit Verification

Experiments of the Expansion of a Colloidal Suspension. We tested experimentally the expansion of a colloidal suspension. Our findings indicate that despite the presence of thermal motion of the individuals, the collective dynamics adhere to an athermal compact expansion. To achieve this, we used optical tweezers to concentrate the particles, following which we turned off the light and monitored the spreading of the colloidal drop (see Fig. 4). Most commonly, optical tweezers have the laser light first enter the objective rear lens, coming to a tight focus at the imaging plane [52]. This creates a strong yet small trap that can typically host a single colloidal particle ($\sim 1 \mu\text{m}$). To make a trap that can corral many particles, we built a custom optical setup by using a nearly collimated laser beam that first passes through the sample, and only then enters the objective

through the collecting lens [53–55] (see Methods and SI for further details). We used $d = 3 \mu\text{m}$ colloidal particles suspended in deionized water. The particles are charge-stabilized, repel through screened Coulomb interaction, and can be approximated using the DLVO theory to follow $U(r) \propto \exp\{d/l - r/l\}/r$, where l can be approximated from the Debye screening length, $l \approx \lambda_D + d/2$, and $\lambda_D \approx 1 \mu\text{m}$ [56]. With no light, individual particles display Brownian motion with a measured diffusion constant of $D_0 = 0.11 \pm 0.02 \mu\text{m}^2/\text{s}$ (see Supporting Information).

When the laser is turned on, particles are softly attracted into the region of a higher optical field, collecting approximately $N \approx 10^4$ particles (see Fig. 4A). Particles are packed at an effective area fraction of 0.9. Given the individual diffusion constant, the effective area fraction, and the Debye screening length, the suspension is expected to be in the semi-sparse regime ($n < 1$) described in Eq. 2, but above the diffusive regime. Once the beam is turned off, the suspension starts to spread. During the initial half hour of spreading, the suspension remains compact with a sharp boundary. At later times, the boundary turns diffusive, and the expansion is no longer compact (see supporting Movie 1). We measure the size of the drop in the compact expansion regime by thresholding the movie (Fig. 4) and extracting the radius of the drop at each frame. We find that as predicted by Eq. 2, the suspension expands logarithmically.

Discrete Simulation in the Semi-Sparse Limit.

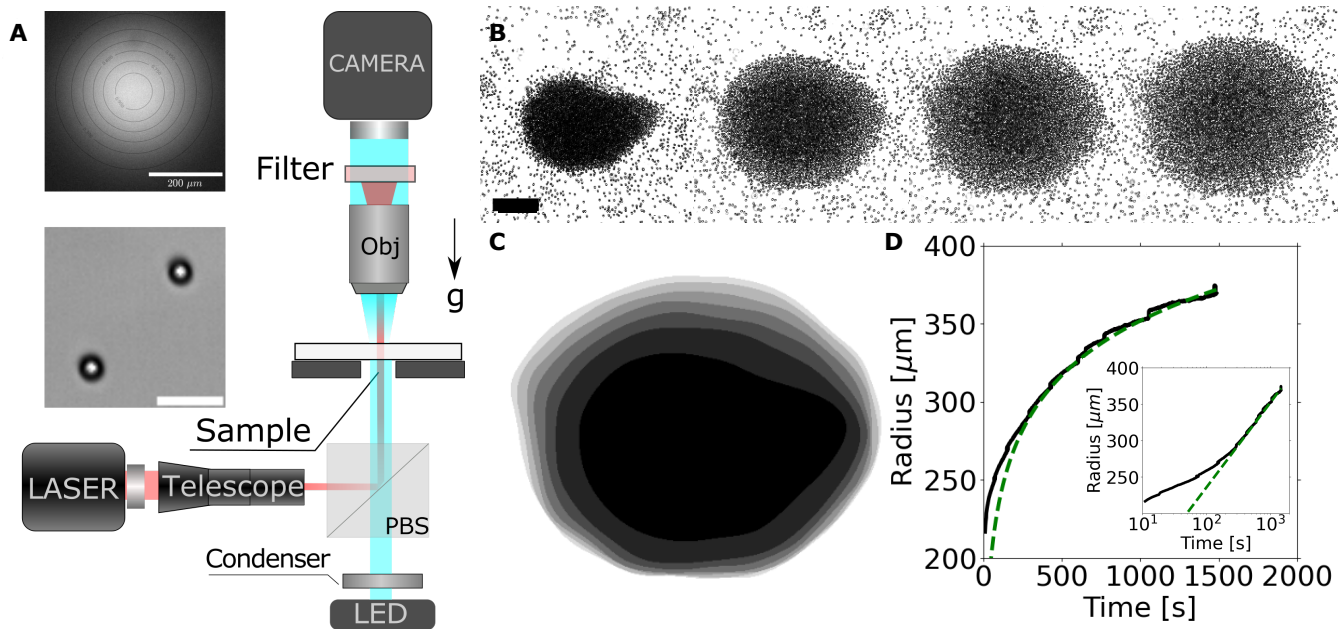


FIG. 4. Experimental results. (A) Large field optical tweezer setup. Top inset shows the light field intensity distribution of the image of the sample (Scalebar $200 \mu\text{m}$). Bottom inset shows an image of two colloidal particles on the surface (Scalebar $10 \mu\text{m}$). (B) Snapshots of a dense suspension with $N \approx 10^4$ particles show a compact expansion, with particles spreading due to screened electrostatic repulsion. Scalebar $100 \mu\text{m}$ (C) Overlapping figures with a color threshold (D) Drop radius as a function of time. The radius shows a logarithmic dependence (green dashed line) as predicted by the theory for a sparse suspension.

Running simulations of 10,000 particles with exponential repulsion (or screened Coulomb repulsion in the SI) either for very long times or starting from a semi-sparse random configuration, results in a logarithmic growth of the drop's radius as a function of time. Figure 1 shows a transition from $R \sim t^{1/4}$ at early times, as predicted by the self-similar solution, to $\sqrt{N/\pi l} \log(t)$ as predicted in the semi-sparse limit, Eq. 13. Even though the analytic arguments made rough assumptions, namely, taking the average distance between particles as a measure of spacing, the coefficient of the logarithm is correctly predicted. In our case $l = 0.005$ giving $\sqrt{N/\pi l} = 0.28$.

CONCLUSIONS

In this work, we identified and characterized the athermal compact expansion of a repulsive suspension. We presented an analytical theory that captures the microscopic origin of the compact expansion and verified its different limits in both simulations, numerics, and experiments. We identified two regimes where a collection of repulsive particles exhibits subdiffusive dynamics. (1) A dense regime where interactions go beyond nearest neighbors, the radius expands as a power law in time ($R \propto t^{1/4}$), and the density profile is self-similar. (2) A semi-sparse regime where interactions are dominated by nearest neighbor contribution and the radius spreads logarithmically with time ($R \propto \log t$). The crossover

between the two regimes occurs when the distance between particles becomes smaller than the decay length of the repulsive potential. Our analysis applies to cases where inter-particle interactions dominate over diffusion. These are applicable in both inherently athermal ensembles, such as granular matter and large organisms, but also for modeling dense microscopic ensembles, as can be found throughout biology, and may serve to guide the design and synthesis of engineered colloidal matter.

MATERIALS AND METHODS

Simulations. *Discrete simulations* were performed using a 5^{th} order Runge-Kutta scheme while adapting step size according to the distance between particles. Starting from a uniform distribution of 10,000 in a disk of radius 0.1, we let the system evolve according to Eq. 3.

Numerical integration of Eq. 4 together with the full velocity given by Eq. 5 were performed starting with a Gaussian distribution with a standard deviation $\sigma = 0.03$ on a grid of $N \times N = 128 \times 128$, and with a timestep $dt = 1/N^2$. In each time step, we calculated the velocity using convolution in Fourier space of Eq. 5 while ensuring the convolution is well behaved by adding padded arrays. The spatial part of the partial differential equation was solved using FFT, whereas the chosen time integration scheme is Leapfrog. We propagated the dynamics over $t = 32,000$ timesteps.

Experiments. To concentrate the particles using optical tweezers, a custom Galilean telescope was used to shrink a 3 mm IR laser source (1064 nm IPG Photonics) into a

nearly collimated beam with a diameter of $D \approx 300 \mu\text{m}$ at the sample (see Fig. 4A). We used $d = 3 \mu\text{m}$ colloidal particles (Bangslabs) suspended in deionized water (Millipore, 18.2M Ωcm), with $\text{pH} \approx 6.3$. The suspension was loaded into a $100 \mu\text{m}$ tall, passivated capillary glass (Vitrotubes, see SI for treatment details). Particles settle at the bottom surface and form a quasi-2D suspension (gravitational height $h_g \approx 20\text{nm} < 0.01d$) with a filling fraction of $\varphi = Nd^2/D^2 \lesssim 0.9$. Note that despite being in a high filling fraction ($\varphi \lesssim 1$), the expansion follows the semi-sparse limit, as $l \lesssim d$.

Author Contribution. NO derived the theory, and developed the molecular dynamics simulations. MYBZ performed experiments. Both authors wrote the numerical integration code, analyzed the data, and wrote the manuscript.

Acknowledgments. We thank Michael Shelley, Haim Diamant, and Philip Rosenau for insightful discussions.

* naomiop@gmail.com

- [1] J. C. Crocker and D. G. Grier, *MRS Bulletin* **23**, 24 (1998).
- [2] C. N. Likos, *Physics Reports* **348**, 267 (2001).
- [3] D. A. Walker, B. Kowalczyk, M. O. de La Cruz, and B. A. Grzybowski, *Nanoscale* **3**, 1316 (2011).
- [4] Y. Hu, P. M. Vlahovska, and M. J. Miksis, *Mathematical Biosciences and Engineering* **18** (2021).
- [5] J. J. Sieber, K. I. Willig, C. Kutzner, C. Gerding-Reimers, B. Harke, G. Donnert, B. Rammner, C. Eggeling, S. W. Hell, H. Grubmüller, *et al.*, *Science* **317**, 1072 (2007).
- [6] F. B. Sheinerman, R. Norel, and B. Honig, *Current opinion in structural biology* **10**, 153 (2000).
- [7] N. Oppenheimer, D. B. Stein, and M. J. Shelley, *Physical review letters* **123**, 148101 (2019).
- [8] B. Sorkin and H. Diamant, *Biophysical Journal* **120**, 2030 (2021).
- [9] T. H. Anderson, S. H. Donaldson, H. Zeng, and J. N. Israelachvili, *Langmuir* **26**, 14458 (2010).
- [10] P. M. Vlahovska, *Annual Review of Fluid Mechanics* **51**, 305 (2019).
- [11] D. R. Link, E. Grasland-Mongrain, A. Duri, F. Sarrazin, Z. Cheng, G. Cristobal, M. Marquez, and D. A. Weitz, *Angewandte Chemie International Edition* **45**, 2556 (2006).
- [12] J. Crow, P. Auer, and J. Allen, *Journal of Plasma Physics* **14**, 65 (1975).
- [13] J. P. Freidberg, *Cambridge University Press*, Vol. 1 (2007) p. 671, arXiv:arXiv:1011.1669v3.
- [14] M. Li, J. Lu, Z. Chen, and K. Amine, *Advanced Materials* **30**, 1 (2018).
- [15] A. Y. U. Grosberg and A. R. Khokhlov, *Statistical Physics of Macromolecules* (American Institute of Physics, 1994) p. 351.
- [16] S. Milner, T. A. Witten, and M. E. Cates, *Macromolecules* **21**, 2610 (1988).
- [17] B. M. Mladek, P. Charbonneau, C. N. Likos, D. Frenkel, and G. Kahl, *Journal of Physics: Condensed Matter* **20**, 494245 (2008).
- [18] H. D. Young, R. A. Freedman, and A. Lewis Ford, *University Physics with Modern Physics Technology Update: Pearson International Edition* (2013) p. 1744.
- [19] R. A. LaCour, C. S. Adorf, J. Dshemuchadse, and S. C. Glotzer, *ACS nano* **13**, 13829 (2019).
- [20] H. M. Jaeger, S. R. Nagel, and R. P. Behringer, *Reviews of Modern Physics* **68**, 1259 (1996).
- [21] A. Baskaran and M. C. Marchetti, *Proceedings of the National Academy of Sciences* **106**, 15567 (2009).
- [22] C. Bechinger, R. Di Leonardo, H. Löwen, C. Reichhardt, G. Volpe, and G. Volpe, *Reviews of Modern Physics* **88**, 045006 (2016), arXiv:1602.00081.
- [23] H. Ko, T. Y. Yu, and D. L. Hu, *Bioinspiration and Biomimetics* **17** (2022), 10.1088/1748-3190/ac6d98.
- [24] O. Peleg, J. M. Peters, M. K. Salcedo, and L. Mahadevan, *Nature Physics* **14**, 1193 (2018).
- [25] C. W. Reynolds, in *Proceedings of the 14th annual conference on Computer graphics and interactive techniques - SIGGRAPH '87*, July (ACM Press, New York, New York, USA, 1987) pp. 25–34.
- [26] D. Helbing, L. Buzna, A. Johansson, and T. Werner, *Transportation Science* **39**, 1 (2005).
- [27] K. A. Bacik, B. S. Bacik, and T. Rogers, *Science* **379**, 923 (2023).
- [28] J. L. Silverberg, M. Bierbaum, J. P. Sethna, and I. Cohen, *Physical Review Letters* **110**, 1 (2013).
- [29] G. S. Redner, M. F. Hagan, and A. Baskaran, *Phys Rev Lett* **110**, 055701.
- [30] M. E. Cates and J. Tailleur, *Annu. Rev. Condens. Matter Phys.* **6**, 219 (2015).
- [31] A. P. Solon, J. Stenhammar, R. Wittkowski, M. Kardar, Y. Kafri, M. E. Cates, and J. Tailleur, *Physical review letters* **114**, 198301 (2015).
- [32] K. Yeo, E. Lushi, and P. M. Vlahovska, *Physical review letters* **114**, 188301 (2015).
- [33] N. Oppenheimer, D. B. Stein, M. Y. Ben Zion, and M. J. Shelley, *Nature Communications* **13**, 804 (2022), arXiv:2103.00296.
- [34] L. Tociu, G. Rassolov, É. Fodor, and S. Vaikuntanathan, *The Journal of Chemical Physics* **157** (2022).
- [35] S. Martiniani, P. M. Chaikin, and D. Levine, *Physical Review X* **9**, 11031 (2019), arXiv:1708.04993.
- [36] A. Deblais, T. Barois, T. Guerin, P. H. Delville, R. Vaudaine, J. S. Lintuvuori, J. F. Boudet, J. C. Baret, and H. Kellay, *Physical Review Letters* **120**, 188002 (2018).
- [37] M. Y. Ben Zion, J. Fersula, N. Bredeche, and O. Dauchot, *Science Robotics* **8**, 1 (2023).
- [38] G. I. Barenblatt, *Prikl. Mat. Makh.* **16**, 67 (1952).
- [39] R. Pattle, *The Quarterly Journal of Mechanics and Applied Mathematics* **12**, 407 (1959).
- [40] H. Stone, in *Nonlinear PDE's in Condensed Matter and Reactive Flows* (Springer, 2002) pp. 297–312.
- [41] L. G. Leal, *Advanced transport phenomena: fluid mechanics and convective transport processes*, Vol. 7 (Cambridge University Press, 2007).
- [42] Z. Zhao, L. Li, and Z. Feng, *Mathematical Methods in the Applied Sciences* (2021).
- [43] P. Rosenau and J. M. Hyman, *Physical Review Letters* **70**, 564 (1993).
- [44] H. Yukawa, *Proceedings of the Physico-Mathematical Society of Japan. 3rd Series* **17**, 48 (1935).
- [45] P. Atkins, J. de Paula, and J. Keeler, *Atkins' Physical Chemistry 11th Edition*, 11th ed. (Oxford University Press, Oxford, 2018) p. 940.
- [46] P. M. Chaikin and T. C. Lubensky, *Principles of Condensed Matter Physics* (Cambridge University Press,

- 1995) p. 720.
- [47] B. U. Felderhof, *Journal of Physics A: Mathematical and General* **11**, 929 (1978).
- [48] D. S. Dean, *Journal of Physics A: Mathematical and General* **29**, L613 (1996).
- [49] N. Martzel and C. Aslangul, *Journal of Physics A: Mathematical and General* **34**, 11225 (2001).
- [50] M. Bruna, S. J. Chapman, and M. Robinson, *SIAM Journal on Applied Mathematics* **77**, 2294 (2017).
- [51] As a side comment, if the velocity has a rotational component such that $\mathbf{v}(\mathbf{r}) = \mathbf{v}_r(\mathbf{r})\hat{r} + \mathbf{v}_\theta(\mathbf{r})\hat{\theta}$, that is the rotational component of the velocity, $\mathbf{v}_\theta = v_\theta(r)\hat{\theta}$ is solely a function of r , the rotational part is incompressible $\nabla \cdot \mathbf{v}_\theta = 0$. Therefore, the radial part of the velocity is the only contributor to the density variations.
- [52] A. Ashkin, *Physical Review Letters* **24**, 156 (1970).
- [53] M. Y. Ben Zion, Y. Caba, R. Sha, N. C. Seeman, and P. M. Chaikin, *Soft Matter* **16**, 4358 (2020).
- [54] M. Y. Ben Zion, Y. Caba, A. Modin, and P. M. Chaikin, *Nature Communications* **13**, 184 (2022), arXiv:2012.15087.
- [55] A. Modin, M. Y. Ben Zion, and P. M. Chaikin, *Nature Communications* **14**, 4114 (2023), arXiv:2203.11051.
- [56] M. Doi, *Soft Matter Physics* (Oxford University Press, Oxford, 2013) p. 272.